Role of pair-vibrational correlations in forming the odd-even mass difference

K. Neergård
Fjordtoften 17, 4700 Næstved, Denmark

I. Bentley
Department of Chemistry and Physics, Saint Mary's College, Notre Dame, Indiana 46556, USA

(Received 23 January 2019; published 14 May 2019)

In the random-phase-approximation–amended (RPA-amended) Nilsson–Strutinskij method of calculating nuclear binding energies, the conventional shell correction terms derived from the independent-nucleon model and the Bardeen–Cooper–Schrieffer pairing theory are supplemented by a term which accounts for the pair-vibrational correlation energy. This term is derived by means of the RPA from a pairing Hamiltonian which includes a neutron-proton pairing interaction. The method was used previously in studies of the pattern of binding energies of nuclei with approximately equal numbers N and Z of neutrons and protons and even mass number $A = N + Z$. Here it is applied to odd-A nuclei. Three sets of such nuclei are considered: (i) the sequence of nuclei with $Z = N - 1$ and $25 \leqslant A \leqslant 99$; (ii) the odd-$A$ isotopes of In, Sn, and Sb with $46 \leqslant N \leqslant 92$; (iii) the odd-$A$ isotopes of Sr, Y, Zr, Nb, and Mo with $60 \leqslant N \leqslant 64$. The RPA correction is found to contribute significantly to the calculated odd-even mass differences, particularly in the light nuclei. In the upper *sd* shell this correction accounts for almost the entire odd-even mass difference for odd Z and about half of it for odd N. The size and sign of the RPA contribution varies, which is explained qualitatively in terms of a closed expression for a smooth RPA counter term.

DOI: 10.1103/PhysRevC.99.054315

I. INTRODUCTION

Nuclear binding energies are often calculated in mean-field approximations. The Bardeen–Cooper–Schrieffer (BCS) theory of superconductivity [1], which was applied extensively to the description of pairing in nuclei since its adaption to the nuclear system by Bohr, Mottelson, and Pines [2], Bogolyubov [3], and Solov'yov [4], is such an approximation. Residual interactions, which are neglected in a mean-field approximation, induce *correlations*, which increase the binding energy. We call this extra binding energy the *correlation energy* (in Ref. [5] this term is used differently). The BCS theory, in particular, may be derived, for a given type of fermion (electron, neutron, proton), from the Hamiltonian

$$H = \sum_k \epsilon_k a_k^\dagger a_k - G P^\dagger P, \quad P = \frac{1}{2} \sum_k a_{\bar{k}} a_k. \tag{1}$$

Here a_k annihilates a fermion in a member $|k\rangle$ of an orthonormal set of single-fermion states which is preserved up to phases under time reversal, denoted by the bar. The single-fermion energies $\epsilon_k = \epsilon_{\bar{k}}$ and the coupling constant G are parameters. The second term in the expression (1) is known as the *pairing interaction*. The exact minimum of the Hamiltonian (1) can be calculated with any wanted accuracy for fairly large single-fermion spaces [6]. Figure 1 shows the result of such a calculation in comparison with that obtained when the correlation energy is calculated in the random-phase approximation (RPA) [7]. This approximation is seen to give a good agreement with the exact value. Appreciable deviations only occur in a narrow interval of G about the threshold $G_{\rm cr}$ of BCS pairing. Because the RPA equations derived from the Hamiltonian (1) describe oscillations of the pair field P about the mean-field equilibrium, the correlations may thus be seen as mainly *pair vibrational*.

Calculations of binding energies by the Strutinskij method [8] conventionally include a pairing term based on the BCS theory. Figure 1 indicates a significance of the correlation energy which suggests that it be taken into account. For $G < G_{\rm cr}$, in particular, the pairing interaction induces only correlation energy. Moreover, isobaric invariance requires that the sum of neutron and proton pairing interactions be generalized to

$$-G\vec{P}^\dagger \cdot \vec{P}, \tag{2}$$

with a pair field isovector

$$\vec{P} = i\sqrt{2} \sum_{kl} \langle \bar{l} | t_y \vec{t} \, | k \rangle a_l a_k. \tag{3}$$

Here $\vec{t} = (t_x, t_y, t_z)$ is the single-nucleon isospin, and time reversal is assumed to commute with t_x and t_z and anticommute with t_y. In Eq. (3) the set k or l of quantum numbers includes an eigenvalue of t_z, and the span of the orthonormal set of states $|k\rangle$ is isobarically invariant. The interaction (2) contains a neutron-proton term $-GP_z^\dagger P_z$. In a doubly even nucleus the Hartree–Bogolyubov quasinucleon vacuum derived from the resulting Hamiltonian has $\langle P_z \rangle = 0$ [9], so the neutron-proton interaction also induces only correlation energy.

In a collaboration with Frauendorf we developed an extension of the conventional Nilsson–Strutinskij scheme which

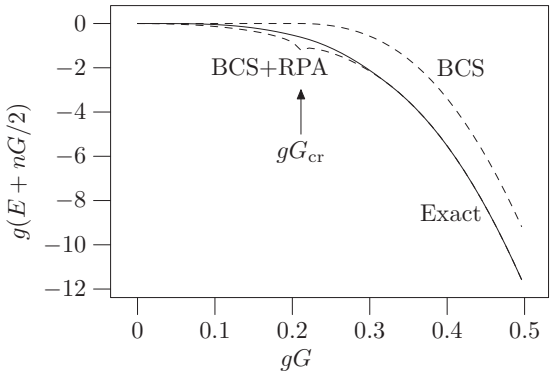

FIG. 1. Adapted from Fig. 1 of Ref. [5]. The exact minimum E of the Hamiltonian (1), normalized to zero for $G = 0$, is shown as a function of G in comparison with the approximations BCS and BCS + RPA. The single-fermion space accommodates 32 equidistant doublet levels $\epsilon_k = \epsilon_{\bar{k}}$ spaced by $1/g$ and is inhabited by $n = 32$ fermions. The expectation value $-Gn/2$ of the pairing interaction in the $G = 0$ ground state is subtracted from the exact and RPA energies. The threshold $G_{\rm cr}$ of BCS pairing is indicated. We turned the figure upside down to display energy rather than binding energy.

takes the pair-vibrational correlations into account in the RPA [10]. Minor modifications of the scheme of calculations proposed in Ref. [10] were discussed by Neergård [11,12]. These articles deal with nuclei with $N \approx Z$ and even A, where N and Z are the numbers of neutrons and protons and $A = N + Z$. The extended Nilsson–Strutinskij scheme was found to account, with suitably chosen parameters, quite well for the pattern of even-A binding energies and certain excitation energies in doubly odd nuclei in this region. We here apply it to odd-A nuclei. We examine in particular the influence of the inclusion of the RPA term on the calculated odd-even mass differences. Three regions of the chart of nuclei are considered: (i) the $N \approx Z$ region, previously studied with respect to the even-A nuclei; (ii) a neighborhood of the Sn isotopic chain; (iii) a region of well-deformed, neutron-rich nuclei around ^{102}Zr.

The organization of the article is as follows: In Sec. II we describe the scheme of calculations. This section serves to present in one place all ingredients of the RPA-amended Nilsson–Strutinskij method in the form it has taken after several modifications since the publication of Ref. [10]. Then, in each of Secs. III–V, we discuss the results for one of the regions (i)–(iii). Finally, after exploring in Sec. VI a technical matter of interpolation of the RPA energy across the threshold of BCS pairing, we summarize our results in Sec. VII.

II. RPA-AMENDED NILSSON–STRUTINSKIJ MODEL

The binding energy $-E(N, Z)$ is calculated by

$$E(N,Z) = E_{\rm LD} + \sum_{\tau=n,p} (\delta E_{\rm i.n.,\tau} + \delta E_{\rm BCS,\tau}) + \sum_{\tau=n,p,np} \delta E_{\rm RPA,\tau}, \tag{4}$$

where "i.n." stands for "independent nucleons." Here $E_{\rm LD}$ is a liquid-drop energy, and each term δE_x has the form

$$\delta E_x = E_x - \tilde{E}_x, \tag{5}$$

with a "smooth" counter term $\tilde{E}_x$. The "microscopic" energy

$$E_{\rm mic} = \sum_{\tau=n,p} (E_{\rm i.n.,\tau} + E_{\rm BCS,\tau}) + \sum_{\tau=n,p,np} E_{\rm RPA,\tau} \tag{6}$$

approximates the minimum of the Hamiltonian

$$H = \sum_{\tau=n,p} \sum_{k=1}^{2\Omega_\tau} \epsilon_{k\tau} a^\dagger_{k\tau} a_{k\tau} - \sum_{\tau=n,p,np} G_\tau P^\dagger_\tau P_\tau, \tag{7}$$

where

$$P_n = \frac{1}{2} \sum_{k=1}^{2\Omega_n} a_{\bar{k}n} a_{kn}, \quad P_p = \frac{1}{2} \sum_{k=1}^{2\Omega_p} a_{\bar{k}p} a_{kp},$$

$$P_{np} = 2^{-\frac{3}{2}} \sum_{k=1}^{2\Omega_{np}} (a_{\bar{k}p} a_{kn} + a_{\bar{k}n} a_{kp}). \tag{8}$$

Here, unlike in Eq. (3), the index k numbers, for each $\tau = n$ for neutrons and $\tau = p$ for protons, an orthonormal set of eigenstates $|k\tau\rangle$ of a time-reversal-invariant single-nucleon Hamiltonian h_τ in an order of nondecreasing eigenvalue $\epsilon_{k\tau}$. The numbering should be such that $|kp\rangle = t_-|kn\rangle$ in the limit $h_p = h_n$. In this limit then $P_n = -P_-/\sqrt{2}$, $P_p = P_+/\sqrt{2}$, and $P_{np} = P_z$ in terms of components of the isovector (3) provided also all Ω_τ are equal. Again the set of states $|k\tau\rangle$ is supposed to be preserved under time reversal up to phases. We also assume that each pair of an odd and the following even k refer to a pair of states connected by time reversal up to phases. Both of these assumptions are satisfied automatically if the eigenvalues are doubly degenerate; that is, except in spherical nuclei. In the spherical case it is satisfied if degenerate orbits are distinguished by a magnetic quantum number m and pairs of an odd and the following even k refer to pairs of states with opposite m.

Unlike Ref. [10] strict isobaric invariance is not imposed on the microscopic model. The single-nucleon Hamiltonians h_n and h_p may be different, and different valence space dimension $2\Omega_\tau$ may be employed for different τ. We use throughout $\Omega_n = N$, $\Omega_p = Z$, and $\Omega_{np} = \lceil A/2 \rceil$ so that the neutron and proton valence spaces are always half filled and $\Omega_{np} \approx (\Omega_n + \Omega_p)/2$. These modifications, which where introduced partly in Refs. [11,12], renders the model better suited for nuclei with a large neutron or proton excess.

We also allow different coupling constants G_τ for different τ, writing

$$G_\tau = \overline{G} A^\zeta (1 - \alpha M_T M'_T), \tag{9}$$

where $M_T = (N - Z)/2$ is the isomagnetic quantum number of the nucleus and M'_T that of the interacting pair; that is, $M'_T = 1$, -1, and 0 for $\tau = n$, p, and np, respectively. The parameters $\overline{G}$, ζ, and α are set separately for each region (i)–(iii). The limit where $h_p = h_n$, all G_τ are equal, and all Ω_τ are equal will be referred to as the *limit of isobaric invariance*.

For each nucleus we assume a deformation, which we take from a conventional Nilsson–Strutinskij calculation [13]. It is

expressed by the Nilsson parameters ϵ_2, γ, and ϵ_4 [14,15]. The deformations are listed in the Appendix.

A. Liquid-drop energy

The liquid-drop energy is written

$$E_{\rm LD} = -\left(a_v - a_{vt}\frac{|M_T|(|M_T|+1)}{A^2}\right)A + \left(a_s - a_{st}\frac{|M_T|(|M_T|+1)}{A^2}\right)A^{2/3}B_s + a_c\frac{Z(Z-1)}{A^{1/3}}B_c, \tag{10}$$

where the coefficients a_x are parameters. The deformation-dependent factors B_s and B_c are calculated from the Nilsson parameters in two steps. First, following Seeger and Howard [16], we determine the coefficients α_{lm} in the equations in spherical coordinates (r,θ,ϕ) of the surfaces of constant second term in the expression (16) below,

$$r \propto 1 + \sum_{|m|\leqslant l>0} (-)^m \alpha_{lm}\sqrt{\frac{(l-|m|)!}{(l+|m|)!}}P_l^{|m|}(\cos\theta)\exp(-im\phi), \tag{11}$$

where $P_l^m(x)$ is the Legendre function of the first kind as defined by Edmonds [17]. With $\epsilon_{20} = \epsilon_2\cos\gamma$ and $\epsilon_{22} = (-\epsilon_2\sin\gamma)/\sqrt{2}$, the nonzero coefficients with $l \leqslant 4$ are given to second order in ϵ_2 and ϵ_4 by

$$\begin{aligned}
\alpha_{20} &= \frac{2}{3}\epsilon_{20} + \frac{5}{63}\epsilon_{20}^2 - \frac{2}{21}\epsilon_{20}\epsilon_4 - \frac{10}{63}\epsilon_{22}^2 + \frac{50}{231}\epsilon_4^2,\\
\alpha_{22} &= \alpha_{2(-2)} = \frac{2}{3}\epsilon_{22} - \frac{10}{63}\epsilon_{20}\epsilon_{22} - \frac{1}{63}\epsilon_{22}\epsilon_4,\\
\alpha_{40} &= -\epsilon_4 + \frac{12}{35}\epsilon_{20}^2 - \frac{30}{77}\epsilon_{20}\epsilon_4 + \frac{4}{35}\epsilon_{22}^2 + \frac{243}{1001}\epsilon_4^2,\\
\alpha_{42} &= \alpha_{4(-2)} = \sqrt{\frac{48}{245}}\epsilon_{20}\epsilon_{22} + \sqrt{\frac{1215}{5929}}\epsilon_{22}\epsilon_4,\\
\alpha_{44} &= \alpha_{4(-4)} = \sqrt{\frac{8}{35}}\epsilon_{22}^2.
\end{aligned} \tag{12}$$

This approximation is adopted. For $\epsilon_{22} = 0$, the expansion (12) (including results for $l > 4$ which we do not show) should give Eqs. (10)–(13) of Ref. [16]. Some coefficients there differ from ours, which were derived by computer algebra.

The coefficients with $l > 4$ are not required in the second step, where B_s and B_c are expanded in the αs. This expansion can be derived from Swiatecki's results in Ref. [18]. Swiatecki's expansion is restricted to $\gamma = 0$, but when only terms of total rank 8 or less are retained, each term has a unique continuation into $\gamma \neq 0$ given by the requirement that it be a scalar polynomial in the spherical tensor components α_{lm}. The resulting expansion, which we adopt, is

$$\begin{aligned}
B_s &= 1 + \tfrac{2}{5}p_{20} - \tfrac{4}{105}p_{30} - \tfrac{66}{175}p_{40} - \tfrac{4}{35}p_{21} + p_{02},\\
B_c &= 1 - \tfrac{1}{5}p_{20} - \tfrac{4}{105}p_{30} + \tfrac{51}{245}p_{40} - \tfrac{6}{35}p_{21} - \tfrac{5}{27}p_{02},
\end{aligned} \tag{13}$$

TABLE I. Liquid-drop parameters for optimal pairing parameters. The last column shows the rms deviation from the data. The unit is MeV throughout.

	a_v	a_{vt}	a_s	a_{st}	a_c	rms
$N \approx Z$	15.23	112.5	16.52	148.9	0.6601	1.018
Around Sn	15.37	115.2	16.97	157.5	0.6737	0.515
Around ^{102}Zr	14.78	151.2	16.07	355.5	0.5774	0.043

with

$$\begin{aligned}
p_{20} &= \alpha_{20}^2 + 2\alpha_{22}^2, \quad p_{30} = \alpha_{20}\left(\alpha_{20}^2 - 6\alpha_{22}^2\right), \quad p_{40} = p_{20}^2,\\
p_{21} &= \left(\alpha_{20}^2 + \frac{1}{3}\alpha_{22}^2\right)\alpha_{40} + \sqrt{\frac{20}{3}}\alpha_{20}\alpha_{22}\alpha_{42} + \sqrt{\frac{70}{9}}\alpha_{22}^2\alpha_{44},\\
p_{02} &= \alpha_{40}^2 + 2\alpha_{42}^2 + 2\alpha_{44}^2.
\end{aligned} \tag{14}$$

For given pairing parameters $\overline{G}$, ζ, α and an RPA interpolation width w defined in Sec. VI we fix the coefficients a_x in Eq. (10) by a least-square fit of the calculated total energies (4) to the measured ones. Included in this fit are all doubly even nuclei in the considered region of the chart of nuclei whose binding energies have been measured. The limits of each region for this purpose are specified in Secs. III–V. The fit of the liquid-drop parameters a_x is done before the pairing parameters are fit to other data. Table I shows the results for the optimal pairing parameters. For the ^{102}Zr region the sample of doubly even nuclei consists of only nine nuclei.

B. Independent nucleons

The terms $E_{\rm i.n.,\tau}$ in Eq. (6) are given by

$$E_{\rm i.n.,\tau} = \sum_{k=1}^{N_\tau}\epsilon_{k\tau}, \tag{15}$$

with $N_\tau = N$ for $\tau = n$ and $N_\tau = Z$ for $\tau = p$. The single-nucleon energies $\epsilon_{k\tau}$ are the eigenvalues of the Nilsson Hamiltonian [14,15,19],

$$h_\tau = \frac{\boldsymbol{p}^2}{2M_\tau} + \frac{1}{2}\left(M_\tau\sum_{q=1}^{3}(\omega_\alpha x_\alpha)^2 + 2\epsilon_4\omega_0\rho^2P_4(\cos\theta_{\rm t})\right) - \kappa_{N_{\rm sh},\tau}\mathring{\omega}\left[2\boldsymbol{l}_{\rm t}\cdot\boldsymbol{s} + \mu_{N_{\rm sh},\tau}\left(\boldsymbol{l}_{\rm t}^2 - \langle\boldsymbol{l}_{\rm t}^2\rangle_{N_{\rm sh}}\right)\right], \tag{16}$$

where $\boldsymbol{r} = (x_1, x_2, x_3)$ and $\boldsymbol{p}$ are the spatial coordinates and momentum, $\boldsymbol{s}$ is the spin, and M_τ is the nucleon mass. The function $P_l(x)$ is the Legendre polynomial. The oscillator frequencies ω_q are given by

$$\omega_q = \omega_0\left[1 - \frac{2}{3}\epsilon_2\cos\left(\gamma + q\frac{2\pi}{3}\right)\right], \tag{17}$$

where ω_0 satisfies the condition of volume conservation:

$$\prod_{q=1}^{3}\omega_q = \mathring{\omega}^3, \quad \mathring{\omega} = 41A^{-1/3}\ {\rm MeV}. \tag{18}$$

The "stretched" spherical coordinates $(\rho,\theta_{\rm t},\phi_{\rm t})$ and orbital angular momentum $\boldsymbol{l}_{\rm t}$ [19] correspond to Cartesian

coordinates

$$\xi_{q\tau} = x_q\sqrt{M_\tau\omega_q}, \tag{19}$$

and $N_{\rm sh}$ is the number of oscillator quanta. For the parameters $\kappa_{N_{\rm sh},\tau}$ and $\mu_{N_{\rm sh},\tau}$ we adopt the values recommended in Ref. [20].

The independent-nucleon counter terms are

$$\tilde{E}_{\rm i.n.,\tau} = 2\int_{-\infty}^{\tilde{\lambda}_\tau} \epsilon\tilde{g}_\tau(\epsilon)d\epsilon, \tag{20}$$

where the smooth chemical potential $\tilde{\lambda}_\tau$ is defined by

$$2\int_{-\infty}^{\tilde{\lambda}_\tau} \tilde{g}_\tau(\epsilon)d\epsilon = N_\tau, \tag{21}$$

and the smooth level density $\tilde{g}_\tau(\epsilon)$ is given by [8,21]

$$\tilde{g}_\tau(\epsilon) = \frac{1}{2\gamma_{\rm Str}\sqrt{\pi}}\sum_k L\left(m_{\rm Str}, \frac{1}{2}, \left(\frac{\epsilon-\epsilon_{k\tau}}{\gamma_{\rm Str}}\right)^2\right) \times \exp\left[-\left(\frac{\epsilon-\epsilon_{k\tau}}{\gamma_{\rm Str}}\right)^2\right] \tag{22}$$

in terms of the generalized Laguerre polynomial $L(n,a,x)$. We use smoothing width $\gamma_{\rm Str} = \mathring{\omega}$ and smoothing order $m_{\rm Str} = 3$ and include in the sum in Eq. (22) all such k that $\epsilon_{k\tau} < 47.5\ {\rm MeV} + 5\,\gamma_{\rm Str}$ and $N_{\rm sh} \leqslant 9$.

C. BCS theory

The terms $E_{{\rm BCS},\tau}$ are given by the standard BCS theory. A derivation of the following equations is found, for example in Ref. [9]. For even N_τ one has

$$E_{{\rm BCS},\tau} = \sum_{k=1}^{2\Omega_\tau} v_{k\tau}^2\epsilon_{k\tau} - \frac{\Delta_\tau^2}{G_\tau} - E_{\rm i.n.,\tau}, \tag{23}$$

with

$$\left.\begin{matrix} u_{k\tau} \\ v_{k\tau}\end{matrix}\right\} = \sqrt{\frac{1}{2}\left(1 \pm \frac{\epsilon_{k\tau}-\lambda_\tau}{E_{k\tau}}\right)}, \quad E_{k\tau} = \sqrt{(\epsilon_{k\tau}-\lambda_\tau)^2+\Delta_\tau^2}. \tag{24}$$

Here λ_τ and Δ_τ obey

$$\sum_{k=1}^{2\Omega_\tau} v_{k\tau}^2 = N_\tau, \quad G_\tau\sum_{k=1}^{2\Omega_\tau} u_{k\tau}v_{k\tau} = 2\Delta_\tau. \tag{25}$$

For later reference we define the quasinucleon annihilators

$$\alpha_{k\tau} = u_{k\tau}a_{k\tau} - v_{k\tau}a_{\bar{k}\tau}^\dagger. \tag{26}$$

The equations (24) and (25) always have a solution with $\Delta_\tau = 0$ and there is a threshold $G_{{\rm cr},\tau}$ such that no other Δ_τ is possible for $G \leqslant G_{{\rm cr},\tau}$. For $G > G_{{\rm cr},\tau}$ there is a solution with $\Delta_\tau > 0$ and a lower $E_{{\rm BCS},\tau}$, which is chosen. If $\epsilon_{(N_\tau+2)\tau} > \epsilon_{N_\tau\tau}$ then $G_{{\rm cr},\tau} > 0$ and $G_{{\rm cr},\tau}$ is given by

$$\frac{4}{G_{{\rm cr},\tau}} = \min_{\epsilon_{N_\tau\tau}<\lambda_\tau<\epsilon_{(N_\tau+2)\tau}} \sum_{k=1}^{2\Omega_\tau}\frac{1}{|\epsilon_{k\tau}-\lambda_\tau|}. \tag{27}$$

If $\epsilon_{(N_\tau+2)\tau} = \epsilon_{N_\tau\tau}$, as happens in spherical nuclei when a j shell is partly occupied in the absence of pairing, then $G_{{\rm cr},\tau} = 0$.

If N_τ is odd, a Bogolyubov quasinucleon annihilated by $\alpha_{N_\tau\tau}$ is assumed to be present in the BCS ground state. The orbit $|N_\tau\tau\rangle$ is then fully occupied and its time reverse $|(N_\tau+1)\tau\rangle$ fully empty. The BCS energy $E_{{\rm BCS},\tau}$ is calculated as if $N_\tau - 1$ nucleons of type τ inhabited the remaining orbits. The odd nucleon is said to *block the Fermi level*.

To simplify notation we let $\tilde{g}_\tau$ without an argument mean $\tilde{g}_\tau(\tilde{\lambda}_\tau)$ and write

$$\frac{1}{\tilde{g}_\tau G_\tau} = \chi_\tau. \tag{28}$$

The BCS counter terms are then given by [11,22]

$$\tilde{E}_{{\rm BCS},\tau} = -\frac{1}{2}\Omega_\tau\tilde{\Delta}_\tau\exp(-\chi_\tau), \quad \tilde{\Delta}_\tau = \frac{\Omega_\tau}{2\tilde{g}_\tau\sinh\chi_\tau}. \tag{29}$$

D. Random-phase approximation

The calculation of $E_{{\rm RPA},\tau}$ is based on the theory in Ref. [9]. It involves linear relations in the space spanned by the terms in the sums in Eq. (8). A linearly independent set of terms in the expression for P_τ may be labeled by the odd single-nucleon indices k from 1 to $2\Omega_\tau - 1$. When both N and Z are even, we denote this set of k by $\mathcal{S}_\tau$. Modifications of this definition when one or both of N and Z are odd are discussed below. It is convenient to introduce at this point labels $\tau\tau' = nn, pp, np$ alternative to and synonymous with $\tau = n, p, np$ and vectors and matrices with components or element indexed by the set $\mathcal{S}_{\tau\tau'}$. A diagonal matrix $\mathsf{E}_{\tau\tau'}$ is defined by its elements

$$E_{\tau\tau',kl} = \delta_{kl}(E_{k\tau} + E_{k\tau'}) \tag{30}$$

and column vectors $\mathsf{U}_{\tau\tau'}$ and $\mathsf{V}_{\tau\tau'}$ by their components

$$U_{\tau\tau',k} = u_{k\tau}u_{k\tau'}, \quad V_{\tau\tau',k} = -v_{k\tau}v_{k\tau'}. \tag{31}$$

Let

$$\mathsf{A}_{\tau\tau'} = \mathsf{E}_{\tau\tau'} - G_{\tau\tau'}(\mathsf{U}_{\tau\tau'}\mathsf{U}_{\tau\tau'}{}^T + \mathsf{V}_{\tau\tau'}\mathsf{V}_{\tau\tau'}{}^T),$$
$$\mathsf{B}_{\tau\tau'} = -G_{\tau\tau'}(\mathsf{U}_{\tau\tau'}\mathsf{V}_{\tau\tau'}{}^T + \mathsf{V}_{\tau\tau'}\mathsf{U}_{\tau\tau'}{}^T). \tag{32}$$

Then

$$E_{{\rm RPA},\tau\tau'} = \frac{1}{2}\left(\sum_k\sqrt{z_{\tau\tau',k}} - {\rm tr}\,\mathsf{E}_{\tau\tau'}\right), \tag{33}$$

where $z_{\tau\tau',k}$ are the eigenvalues of

$$(\mathsf{A}_{\tau\tau'} + \mathsf{B}_{\tau\tau'})(\mathsf{A}_{\tau\tau'} - \mathsf{B}_{\tau\tau'}). \tag{34}$$

The terms $\sqrt{z_{\tau\tau',k}}$ are the RPA frequencies.

For $\tau = \tau'$ and, in the limit of isobaric invariance, for $\tau\tau' = np$ and $N = Z$, one RPA mode is, for $G_{\tau\tau'} > G_{{\rm cr},\tau\tau'}$ (with $G_{{\rm cr},np} = G_{{\rm cr},n} = G_{{\rm cr},p}$ in the isobarically invariant limit), a Nambu–Goldstone mode with zero frequency [9,23]. That is, in this degree of freedom vibration turns into rotation. This is what gives rise to the singularity at $G = G_{\rm cr}$ in Fig. 1 [10]. To circumvent this singularity we interpolate the calculated $E_{{\rm RPA},\tau\tau'}$ across the region of $G_{\tau\tau'} = G_{{\rm cr},\tau\tau'}$ for $\tau = \tau'$ or $\tau\tau' = np$ and $N = Z$ with $G_{{\rm cr},np} \approx G_{{\rm cr},n} \approx G_{{\rm cr},p}$ in the latter case. Details are given in Sec. VI.

The expression (33) results from the expansion of the ground-state energy in Feynman diagrams formed as closed bubble chains; see Eq. (36) in Ref. [9]. Each bubble represents a virtual creation and subsequent annihilation of a pair of Bogolyubov quasinucleons. When, say, N is odd, the presence of the unpaired nucleon in the BCS ground state blocks the creation of quasinucleon pairs by the terms in P_n and $P_n^\dagger$ proportional to $\alpha^\dagger_{Nn}\alpha^\dagger_{(N+1)n}$. Therefore $k = N$ should be and is omitted from $\mathcal{S}_n$ for odd N. The remainder exhausts the set of excitations of the BCS ground state mediated by the fields P_n and $P_n^\dagger$.

The case of $\mathcal{S}_{np}$ is more involved for odd N. The fields P_{np} and $P_{np}^\dagger$ have terms proportional to $\alpha^\dagger_{(N+1)n}\alpha^\dagger_{Np}$ and $\alpha^\dagger_{Np}\alpha_{Nn}$, which, respectively, adds a pair of quasinucleons and scatters the quasineutron in the Fermi level orbit into a quasiproton. The latter excitation, in particular, may have negative energy, which inhibits the use of the RPA. Even when the energy is positive, it is small in comparison to that of the genuine two-quasinucleon excitations, which may render the RPA calculation unstable anyway. For $Z = N$ in the limit of isobaric invariance, both these excitations have zero matrix elements when one assumes, as we do (cf. Sec. II E), that the unpaired neutron and the unpaired proton combine to isospin $T = 0$. This allows the use of Eq. (33), omitting $k = N$ from $\mathcal{S}_{np}$ like it is omitted from $\mathcal{S}_n$. To avoid the troubles just described, we have chosen to do so also when Z is even. That is, we generally omit $k = N$ from $\mathcal{S}_n$ and $\mathcal{S}_{np}$ when N is odd, and analogously for odd Z. In physical terms this amounts to extending to the RPA the assumption in the BCS theory with the Fermi level blocked that the unpaired nucleon acts as a spectator to interactions among the paired nucleons in a valence space that excludes the half occupied single-nucleon level. A more satisfactory treatment of the neutron-proton pair vibrational correlations for odd A might be based on the theory of (quasi-) particle-vibration coupling.

For even N and Z the RPA energy as given by Eq. (33) gets contributions from fluctuations of the quasinucleon vacuum in every direction generated by an operator $\alpha^\dagger_{k\tau}\alpha^\dagger_{\overline{k\tau'}} + \alpha^\dagger_{k\tau'}\alpha^\dagger_{\overline{k\tau}}$ with $k \in \mathcal{S}_{\tau\tau'}$. Vaquero, Egido, and Rodríguez take an different path to study pairing fluctuations [24]. A combination of the variances of N and Z is used (for a given deformation) as a generator coordinate to obtain a wave function that describes the distribution of quasinucleon vacua in the single degree of freedom associated with this coordinate. The quasinucleon vacua are generated by the constrained Hartree–Fock–Bogolyubov method with a Gogny two-nucleon interaction.

For the calculation of the RPA counter terms $\tilde{E}_{\mathrm{RPA},\tau\tau'}$ we define $\tilde{g}_{\tau\tau'}(\epsilon)$ by replacing $\epsilon_{k\tau}$ by $(\epsilon_{k\tau} + \epsilon_{k\tau'})/2$ in the expression (22). This definition coincides with Eq. (22) for $\tau = \tau'$. A function $\tilde{\lambda}_{\tau\tau'}(x)$ is defined by

$$2\int_{-\infty}^{\tilde{\lambda}_{\tau\tau'}(x)} \tilde{g}_{\tau\tau'}(\epsilon)d\epsilon = x. \tag{35}$$

In particular $\tilde{\lambda}_{\tau\tau}(N_\tau) = \tilde{\lambda}_\tau$ by Eq. (21). We let $\tilde{g}_{np}$ without an argument mean $\tilde{g}_{np}(\tilde{\lambda}_{np}(A/2))$ and generalize Eq. (28) to

$$\frac{1}{\tilde{g}_{\tau\tau'}G_{\tau\tau'}} = \chi_{\tau\tau'} \tag{36}$$

and the definition of $\tilde{\Delta}_\tau$ in Eq. (29) to

$$\tilde{\Delta}_{\tau\tau'} = \frac{\Omega_{\tau\tau'}}{2\tilde{g}_{\tau\tau'}\sinh\chi_{\tau\tau'}} \times\sqrt{1-\left(\frac{\tilde{g}_{\tau\tau'}(\tilde{\lambda}_{\tau\tau'}(N_\tau)-\tilde{\lambda}_{\tau\tau'}(N_{\tau'}))\tanh\chi_{\tau\tau'}}{\Omega_{\tau\tau'}}\right)^2}. \tag{37}$$

Then $\tilde{E}_{\mathrm{RPA},\tau\tau'}$ is given by [11]

$$\tilde{E}_{\mathrm{RPA},\tau\tau'} = \frac{2\tilde{\Delta}_{\tau\tau'}}{\pi}\int_0^\infty \ln\left(\frac{1}{\chi_{\tau\tau'}}\tanh^{-1}\left\{\left[1+\left(l_{\tau\tau'}^2+x^2\right)^{-1}\right]^{-\frac{1}{2}}\tanh\chi_{\tau\tau'}\right\}\right)dx, \tag{38}$$

with

$$l_{\tau\tau'} = \frac{\tilde{\lambda}_{\tau\tau'}(N_\tau) - \tilde{\lambda}_{\tau\tau'}(N_{\tau'})}{2\tilde{\Delta}_{\tau\tau'}}. \tag{39}$$

E. Isobaric analogs

The scheme presented so far describes states with isospin $T \approx |M_T|$. This relation is satisfied empirically by nearly all ground states. The exception is that for odd $N = Z > 20$ most ground states have $T \approx 1$ while the lowest states with $T \approx 0$ are excited. For odd $N = Z < 20$ the lowest states with $T \approx 1$ are mostly excited. We denote the energies of these $T \approx 1$ states by $E^*(N, Z)$ to distinguish them from the energies of the $T \approx 0$ states. For odd $N = Z$ the $T \approx 1$ states are the isobaric analogs of the ground states of the doubly even nuclei with neutron and proton numbers $(N', Z') = (N + 1, Z - 1)$. Accordingly we set

$$E^*(N,Z) = E(N',Z') + a_c\frac{Z(Z-1)-Z'(Z'-1)}{A^{1/3}}B_c, \tag{40}$$

where B_c is calculated from the deformation of the doubly even nucleus.

III. $N \approx Z$ REGION

Our calculations for even A in the $N \approx Z$ region follow the scheme previously applied in Refs. [10,12]. Again we consider the doubly even nuclei with $24 \leqslant A \leqslant 100$ and $0 \leqslant N - Z \leqslant 10$ and the doubly odd ones with $26 \leqslant A \leqslant 98$ and $N = Z$. Unlike Ref. [12] we use different Ω_τ for different τ and a considerably smaller interval of interpolation of the RPA energies as discussed in Sec. VI. Furthermore, the

deformations were recalculated, all oscillator shells with $N_{\rm sh} \leqslant 9$ being included in the calculation by the scheme of Ref. [13] instead of just four shells close to the neutron or proton Fermi level for $\tau = n$ and p, respectively. For the doubly even nuclei this only changed the deformations of ^{84}Zr and ^{86}Mo, which went from spherical to oblate. For the $T \approx 0$ states of the doubly odd nuclei, the deformations were determined in the prior work by averaging over the deformations of the adjacent doubly even nuclei. In the present work these deformations are calculated independently by blocking the Fermi levels. This resulted in significant changes of the individual deformations, while the overall pattern of variation along the chain of these states remains the same.

Again we set $\alpha = 0$ in Eq. (9) so that one pair coupling constant G covers the cases $\tau = n$, p, and np. The parameters $\overline{G}$ and ζ are fit to the following data for odd $N = Z$.

(1) The $T \approx 0$ doubly-odd–doubly-even mass differences

$$E(N,N) - \tfrac{1}{2}[E(N-1,N-1) + E(N+1,N+1)]. \quad (41)$$

(2) The differences of the lowest energies for $T \approx 1$ and $T \approx 0$; that is,

$$E^*(N,N) - E(N,N). \quad (42)$$

The set of data is the same as in Refs. [10,12] and thus includes extrapolated masses of ^{82}Nb and ^{86}Tc, but all mass data were updated from AME12 [25] to AME16 [26]. Again excitation energies are taken from the Evaluated Nuclear Structure Data File [27]. A least-square fit gives

$$G = 7.196A^{-0.7461}\ \text{MeV}, \quad (43)$$

with a rms deviation of 0.789 MeV. Plotting the $T \approx 0$ doubly-odd–doubly-even mass differences, the $T \approx 0$ to $T \approx 1$ energy splittings, the symmetry energy coefficients, and the "Wigner x" as functions of A results in figures grossly similar to Figs. 6–9 of Refs. [10] and Fig. 1 of Ref. [12]. As for the Wigner x, more detail is given in Sec. VI.

With the parameters thus set we consider the odd-A nuclei with $Z = N - 1$ and $25 \leqslant A \leqslant 99$. The odd-even mass difference $\Delta_{\rm oe}(N,Z)$ is defined as the mass of the odd-A nucleus relative to the average mass of its two doubly even neighbors. The calculated $\Delta_{\rm oe}(N,Z)$ are shown in Fig. 2 in comparison with the data. The model is seen to reproduce the typical size of the measured values. This is remarkable because $\overline{G}$ and ζ were fit not to these data but to *energies in doubly odd nuclei*. This supports an interpretation of the lowest $T \approx 0$ states of such nuclei as essentially two-quasinucleon states.

The figure also displays the individual contributions to the calculated $\Delta_{\rm oe}(N,Z)$ from $E_{\rm LD}$, $\delta E_{\rm i.n.} = \sum_{\tau=n,p} \delta E_{\rm i.n.,\tau}$, $\delta E_{\rm BCS} = \sum_{\tau=n,p} \delta E_{{\rm BCS},\tau}$, and $\delta E_{\rm RPA} = \sum_{\tau=n,p,np} \delta E_{{\rm RPA},\tau}$. The liquid-drop contribution is negative except for $N = 43$ with an average about -0.4 MeV. The contribution from the independent-nucleon shell correction $\delta E_{\rm i.n.}$ fluctuates wildly as a function of N or Z. These fluctuations are reduced by the pairing, which also renders the total $\Delta_{\rm oe}(N,Z)$ mostly positive in accordance with the data. Very low and, for odd N, even

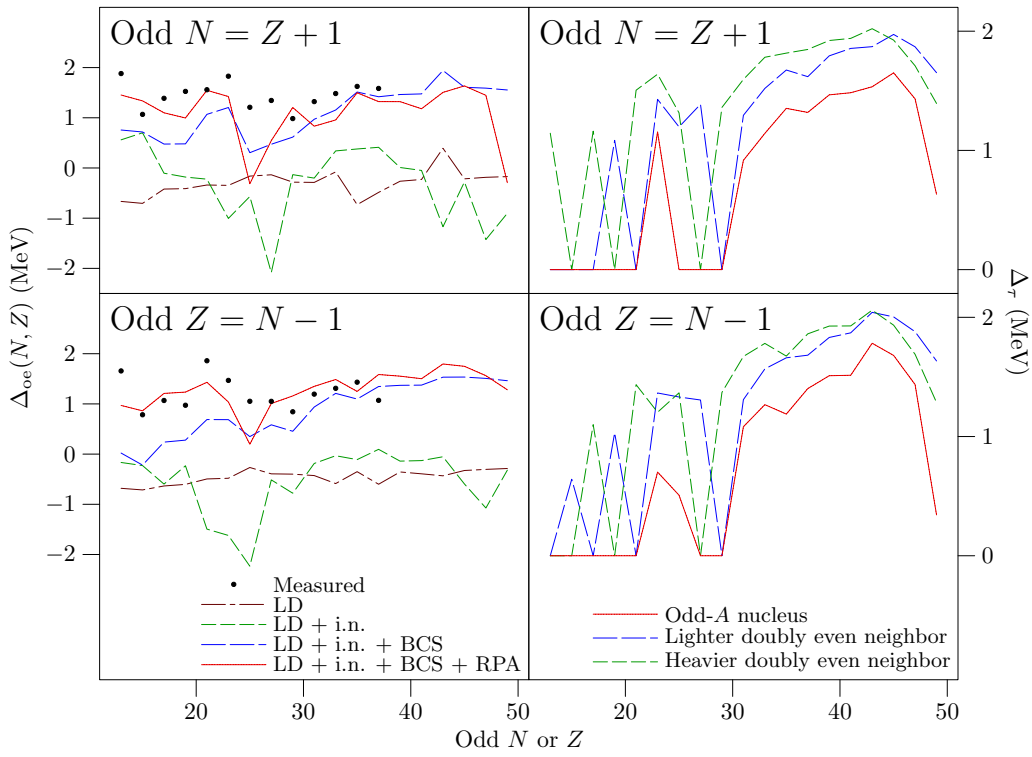

FIG. 2. The panels on the left show the calculated odd-even mass differences $\Delta_{\rm oe}(N,Z)$ for $Z = N - 1$ in successive approximations in comparison with the values extracted from mass data. The panels on the right display the BCS gap parameters Δ_τ of the odd-A nuclei and their doubly even neighbors, where $\tau = n$ for odd N and p for odd Z.

negative values are calculated; however, for N and $Z = 25$ and for $N = 49$, not the least induced by anomalously low contributions of $\delta E_{\rm RPA}$. These low contributions, as well as one at $Z = 49$, are correlated with $G_{{\rm cr},n}$ or $G_{{\rm cr},p}$ being close to G for odd N and Z, respectively, so that the accuracy of the RPA is uncertain (cf. Sec. VI). The measured odd-even mass difference actually decreases when N or $Z = 25$ is approached from below, but this decrease is much exaggerated in the calculation.

The RPA contribution is positive for all odd Z except $Z = 25$ and 49 and for all odd $N < 30$ except $N = 25$. In the upper *sd* shell it gives almost the entire $\Delta_{\rm oe}(N, Z)$ for odd Z and about half of it for odd N. For odd $N > 30$ the RPA contribution is negative, and both for odd N and for odd Z it is numerically smaller in the heavier than in the lighter nuclei.

These differences in the size and sign of the RPA contribution may be understood qualitatively from the expression (38). Thus for $l_{\tau\tau'} = 0$, which holds by Eq. (39) for $\tau = \tau'$ and approximately for $\tau\tau' = np$ and $N \approx Z$, Eqs. (36)–(38) give

$$\tilde{E}_{{\rm RPA},\tau\tau'} = \tfrac{1}{2}\,\Omega_{\tau\tau'} G_{\tau\tau'} f(\chi_{\tau\tau'}), \tag{44}$$

with

$$f(\chi) = \frac{2\chi}{\pi \sinh\chi} \int_0^\infty \times \ln\left(\frac{1}{\chi}\tanh^{-1}[(1+x^{-2})^{-\frac{1}{2}}\tanh\chi]\right) dx. \tag{45}$$

This function is displayed in Fig. 3. The contribution of $\delta E_{\rm RPA}$ to $\Delta_{\rm oe}(N, Z)$ stems mainly from the microscopic term $E_{\rm RPA}$. In fact, because the counter term $\tilde{E}_{\rm RPA}$ is a smooth function of N, Z, and deformation, with no distinction between even and odd N_τ, its contribution is small. Consider the case of odd N. The difference between $E_{{\rm RPA},n\tau}$ for odd and even N is roughly a result of the effective dilution in the odd case of the single-neutron spectrum by the blocking of the Fermi level. The impact on $E_{{\rm RPA},n\tau}$ of this decrease of level density near the Fermi level is similar to the impact on $\tilde{E}_{{\rm RPA},n\tau}$ of a decrease of $\tilde{g}_{n\tau}$. By Eqs. (28) and (36) the latter increases $\chi_{n\tau}$ and thus gives rise to an increase of $\tilde{E}_{{\rm RPA},n\tau}$ proportional to $f'(\chi_{n\tau})$ with a positive coefficient. The case of odd Z is analogous. The calculated $\chi_{\tau\tau'}$ decrease from about 3.8 for $A = 24$ to about 2.6 for $A = 100$. Thus in the lighter nuclei we have $f'(\chi_{\tau\tau'}) > 0$ and accordingly expect a large positive RPA contribution to $\Delta_{\rm oe}(N, Z)$, while in the heavier nuclei we have $f'(\chi_{\tau\tau'}) \approx 0$ and accordingly expect a small contribution, which can take either sign.

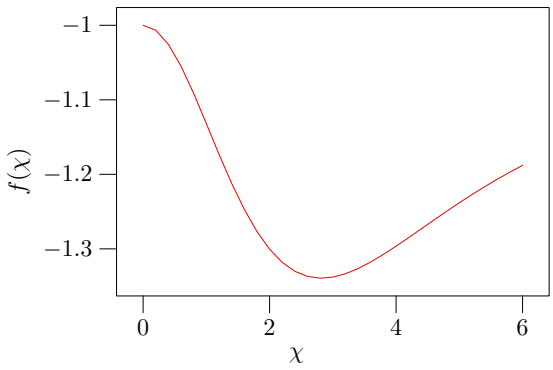

FIG. 3. The function f given by Eq. (45).

Also shown in Fig. 2 are the calculated gap parameters Δ_τ for both the odd-A nucleus and its doubly even neighbors. It is seen that often in the lighter nuclei, $\Delta_\tau = 0$, most often for odd A. The BCS approximation to $\Delta_{\rm oe}(N, Z)$ is seen to follow roughly the fluctuating gap parameters as a function of N or Z.

IV. NEIGHBORHOOD OF THE Sn ISOTOPES

In the neighborhood of the Sn isotopic chain we consider all nuclei with $48 \leqslant Z \leqslant 52$ and even N in the interval $46 \leqslant N \leqslant 92$ and all Sn isotopes with odd N in the interval $47 \leqslant N \leqslant 91$. In Eq. (9), we keep the A exponent $\zeta = -0.7461$ which resulted from the analysis of data for $N = Z$ [cf. Eq. (43)], but adjust $\overline{G}$ and α so as to reproduce the average of the measured $\Delta_{\rm oe}(N, Z)$ separately for odd N and odd Z. The result is

$$G_\tau = 5.818 A^{-0.7461}(1 - 0.0170 M_T M_T')\ {\rm MeV}. \tag{46}$$

For ^{100}Sn, Eq. (43) gives $G_\tau = 0.2317$ MeV for all τ, while Eq. (46) gives $G_\tau = 0.1873$ MeV for all τ. We thus have two determinations of the pair coupling constant in ^{100}Sn, the higher one 24% greater than the lower one. They result from extrapolation from different directions in the chart of nuclei, one from the $N = Z$ line and one from the neighborhood of the Sn isotopic chain. Because the data in the fit (43) include extrapolated masses and interpretations of incomplete spectra of ^{82}Nb and ^{86}Tc, the lower value is likely to be most reliable.

Figure 4 illustrates the need of both the nonzero α and the smaller $\overline{G}$. The quantities plotted in the upper-left, upper-right, and lower-right panels are the total calculated shell correction $\delta E = \delta E_{\rm i.n.} + \delta E_{\rm BCS} + \delta E_{\rm RPA}$ and its empirical counterpart $\delta E_{\rm emp} = E_{\rm emp} - E_{\rm LD}$, where $-E_{\rm emp}$ is the measured binding energy. They are displayed for the doubly even Sn isotopes as functions of N. Different sets of liquid-drop parameters give rise to a difference of $\delta E_{\rm emp}$ between the panels. In the upper-left panel, the pairing parameters are inherited from the $N \approx Z$ region [cf. Eq. (43)]. They describe fairly well the empirical binding energies near the $N = 50$ shell closure but not at all near the $N = 82$ shell closure. Because the Sn isotopes have constant proton configuration, the G_τ that most significantly influences the isotopic variation is G_n. When α is positive, G_n decreases more with increasing N than by the factor $A^{-0.7461}$. The upper-right panel shows the result when $\overline{G} = 7.196$ MeV is kept—so that Eq. (43) would be retained for $N = Z$—but α is set to 0.0170. Now $\delta E_{\rm emp}$ is equally well described at both shell closures, but the empirical $\Delta_{\rm oe}(N, 50)$ is seen in the lower-left panel to be vastly overestimated. The top panel of Fig. 5 shows that this discrepancy is eliminated when $\overline{G}$ is reduced to 5.818 MeV. As seen from the lower-right panel of Fig. 4 this also improves the reproduction of the measured doubly even binding energies near both shell closures.

We notice in passing that, in particular, a discontinuity of the measured two-neutron separation energy at $N = 66$ is reproduced. Togashi *et al.* [28] describe this discontinuity as a second-order phase transition. In our calculations it is

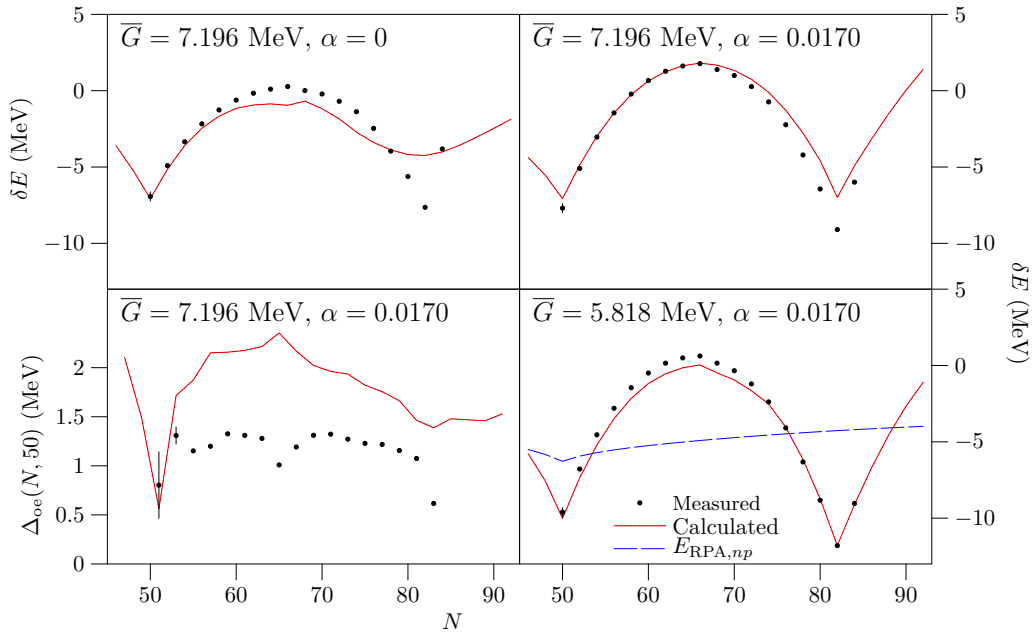

FIG. 4. The upper-left, upper-right, and lower-right panels show the calculated shell corrections δE of the doubly even Sn isotopes for three different sets of pairing parameters. The lower-left panel shows the odd-even mass differences $\Delta_{oe}(N, 50)$ calculated with the pairing parameters of the upper-right panel. For all these results the corresponding empirical values are shown for comparison. The empirical shell corrections δE_{emp} differ between the panels due to different liquid-drop parameters. A plot of the neutron-proton RPA energy $E_{RPA,np}$ is included in the lower-right panel.

correlated with an onset of oblate deformation at the entrance at $N = 68$ of the highly degenerate $1h_{11/2}$ shell (cf. the Appendix). This concurs with a finding of Togashi *et al.*, based on an analysis of the result of a large-scale shell-model calculation, that these nuclei have oblate deformations. In the upper panels of Fig. 4, the plots of δE behave differently at $N \approx 66$. Pairing thus contributes to the formation of the discontinuity in our calculations.

Also shown in Fig. 4 is the neutron-proton RPA energy $E_{RPA,np}(N, 50)$. It increases with increasing neutron excess because the products in Eq. (31) decrease with increasing distance between λ_n and λ_p. It is seen, however, that in ^{142}Sn with almost twice as many neutrons as protons, it is only reduced numerically to about two thirds of its value in the $N = Z$ nucleus ^{100}Sn.

Figure 5 shows the measured and calculated odd-even mass differences and the decompositions of the latter. The RPA contribution to the calculated $\Delta_{oe}(N, Z)$ is positive with few exceptions. On average it makes up 7%, 31%, and 14% of the total for the odd-A isotopes of Sn, In, and Sb. This dominantly positive sign is qualitatively consistent with the values of $\chi_{\tau\tau'}$. For $N = 46$ they are approximately equal, about 3.3, and they decrease slightly to about 3.2 for $N = 54$. When N increases further, χ_n increases to about 4.0 while χ_n and χ_{np} continue decreasing to about 2.7 and 3.0, respectively. That the $\chi_{\tau\tau'}$ of ^{100}Sn are larger here than in the calculation discussed in Sec. III is due to the smaller $\overline{G}$.

Except for the largest N we get $\Delta_\tau = 0$ when N_τ is magic or magic $\pm$ 1. These are the cases when the Fermi level lies within the magic gap in the single-nucleon spectrum. Otherwise $\Delta_\tau > 0$. The emergence of $\Delta_p > 0$ in ^{90}Sn, ^{92}Sn, and ^{92}Sb reflects that $G_{cr,p}$ is close to G_p for the heaviest isotopes of In, Sn, and Sb. This is correlated with low RPA contributions to the calculated $\Delta_{oe}(N, Z)$ in the isotopes of In and Sb with $N = 90$ and 92.

V. ^{102}Zr REGION

In the region around ^{102}Zr we consider all doubly even- and odd-A nuclei with $60 \leqslant N \leqslant 64$ and $38 \leqslant Z \leqslant 42$. As in the Sn region, we keep the A exponent $\zeta = -0.7461$ from Eq. (43) but adjust $\overline{G}$ and α in Eq. (9) so as to reproduce the average of the measured $\Delta_{oe}(N, Z)$ separately for odd N and odd Z. The result is

$$G_\tau = 5.820A^{-0.7461}(1 - 0.0132M_T M'_T)\ \text{MeV}. \quad (47)$$

Thus $\overline{G}$ is practically the same as in the Sn region [cf. Eq. (46)] but α is significantly smaller.

The measured and calculated odd-even mass differences are compared and the decompositions of the latter shown in Fig. 6. The sign of the RPA contribution varies with a slight predominance of the positive sign, which occurs in 8 out of 12 cases. This is consistent with the values of $\chi_{\tau\tau'}$, which are $\chi_n \approx 3.4$ and $\chi_p \approx \chi_{np} \approx 3.2$. On average the RPA contribution makes up 6% of the total calculated $\Delta_{oe}(N, Z)$.

The gap parameters Δ_τ are almost constant with averages about 1.1 MeV for even N and Z and 0.8 MeV for odd A. The latter is close to the average of the calculated $\Delta_{oe}(N, Z)$.

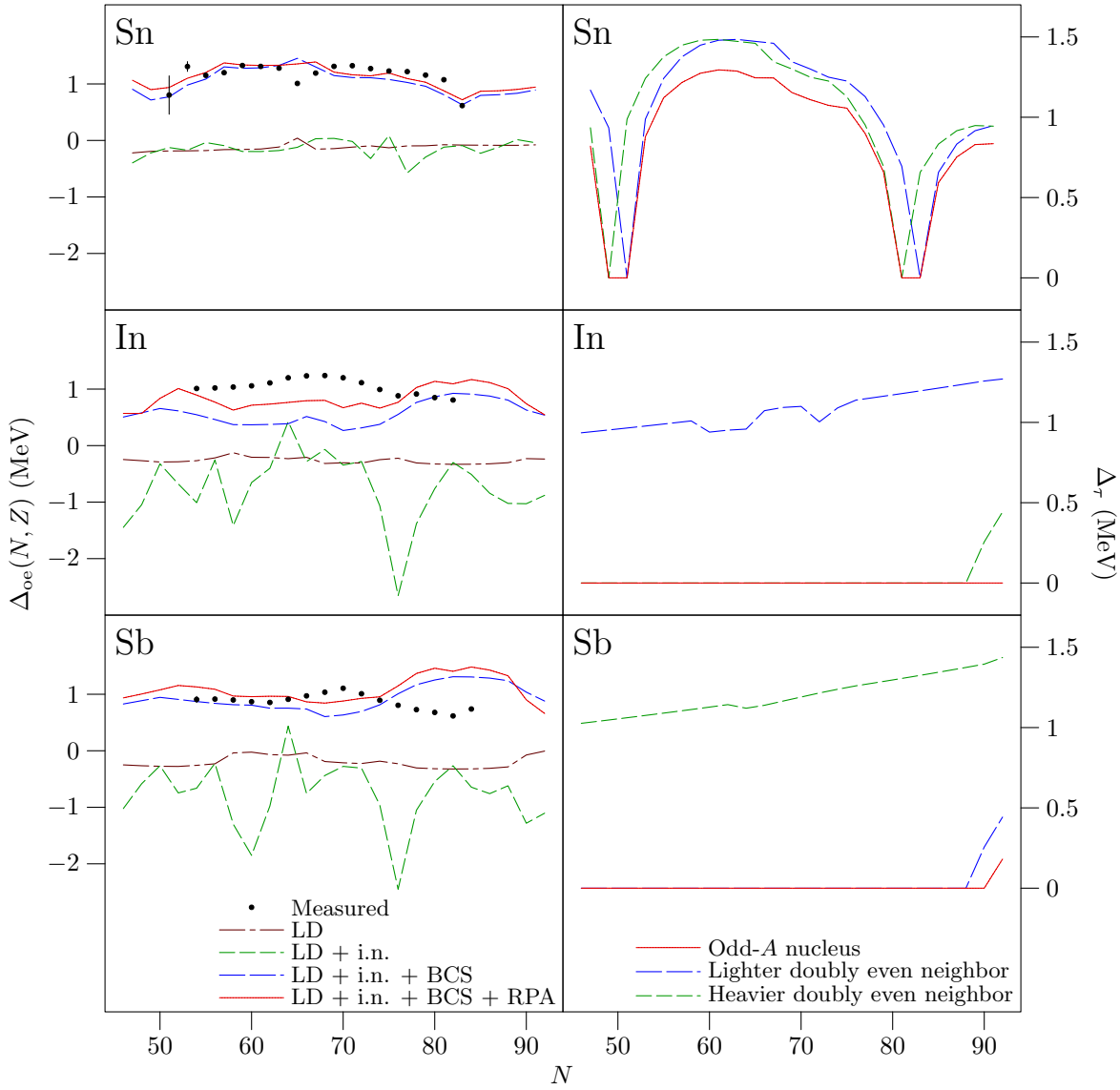

FIG. 5. Similar to Fig. 2 for the neighborhood of the Sn isotopes.

VI. INTERPOLATION

We mentioned that the RPA energies $E_{\mathrm{RPA},\tau\tau'}$ are interpolated across intervals of $G_{\tau\tau'}$ about the thresholds $G_{\mathrm{cr},\tau}$ of BCS pairing to avoid the singularities there. The interpolating function is the polynomial of third degree in $G_{\tau\tau'}$ which joins the calculated values smoothly at the interval endpoints. Interpolation is done for $\tau = \tau'$ and for $\tau\tau' = np$ and $N = Z$. In terms of the interpolation width w mentioned in Sec. II A, the interval is $G_{\mathrm{min},\tau\tau'} < G_{\tau\tau'} < G_{\mathrm{max},\tau\tau'}$ with

$$G_{\mathrm{min},\tau\tau'} = (1-w)\min(G_{\mathrm{cr},\tau}, G_{\mathrm{cr},\tau'}),$$
$$G_{\mathrm{max},\tau\tau'} = (1+w)\max(G_{\mathrm{cr},\tau}, G_{\mathrm{cr},\tau'}). \quad (48)$$

If $G_{\mathrm{max},\tau\tau'} = 0$ no interpolation is done.

For even N_τ the threshold $G_{\mathrm{cr},\tau}$ increases with increasing $\epsilon_{(N_\tau+2)\tau} - \epsilon_{N_\tau\tau}$. It is therefore particularly large when N_τ is magic. As a result both $G_{\mathrm{cr},\tau}$ are close to the common value G of G_n, G_p, and G_{np} in the doubly magic nuclei ^{56}Ni and ^{100}Sn. For ^{100}Sn, Fig. 7 shows the energy E_{mic} given by Eq. (6) as a function of G upon interpolation with different w. A figure for ^{56}Ni is very similar. In this calculation we used the levels $(\epsilon_{kn} + \epsilon_{kp})/2$ for both neutrons and protons so that $G_{\mathrm{cr},n} = G_{\mathrm{cr},p} := G_{\mathrm{cr}}$. It is seen that the choice of w can make a difference of 1–2 MeV in E_{mic} when G_{cr} is close to G.

In Refs. [10,12], $w = 0.5$ was chosen. This choice was based on a comparison with a result of diagonalization of the Hamiltonian (7) in a small valence space [29]. Also, Fig. 1 seems to suggest a fairly large interpolation interval. In the latter calculation, however, the Hamiltonian is given by Eq. (1), not Eq. (7). Probably more importantly, the single-nucleon levels are equidistant. The behavior of the exact energy may be different when the Fermi level lies in a gap in the single-nucleon spectrum. In an early study, Feldman indeed observed an approach of the exact result for the lowest excitation energy to that of the RPA with increasing degeneracies of two separate shells the lower of which is

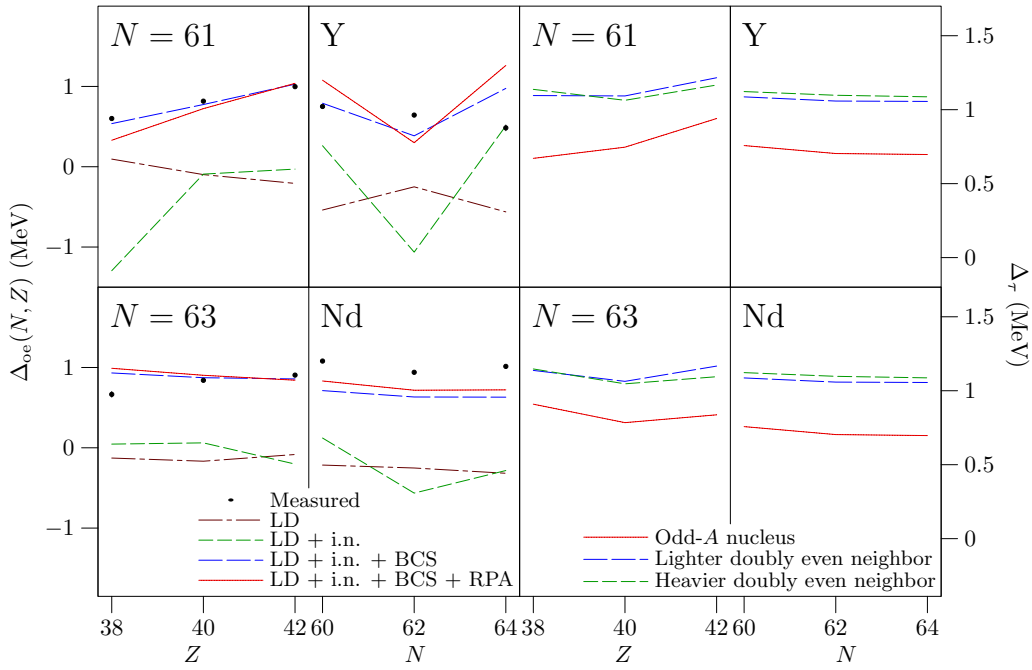

FIG. 6. Similar to Fig. 2 for the neighborhood of ^{102}Zr.

closed for $G = 0$ [30]. There is no way of determining the w which best approximates the exact minimum of any such Hamiltonian other than calibrating the interpolation against an exact calculation, which is beyond our capacity. Dukelsky *et al.* calculated the exact lowest energies for isospin $T = 0$, 1, and 2 given by the Hamiltonian (7) in the limit of isobaric invariance as functions of G for the single nucleus ^{64}Ge with a different valence space and different single-nucleon energies [31], and even in this elaborate calculation the dimension of the valence space (pf shell plus $1g_{9/2}$ subshell) is little greater than half of ours for ^{56}Ni.

With the large w employed in Refs. [10,12], quite a few calculated binding energies depend on this parameter. This is unsatisfactory because the choice of w is largely arbitrary. We prefer to trust the actual RPA energies unless there is a clear reason not to do so. Such a reason is given by the observation that the exact minimum of the Hamiltonian (7) must decrease as a function of G because the interaction is negative definite. As shown in Fig. 7, for the interpolated $E_{\rm mic}$ of ^{100}Sn to similarly decrease as a function of G it is necessary that $w \gtrsim 0.035$. The same approximate limit results for ^{56}Ni. Therefore $w = 0.035$ was used in the present calculations.

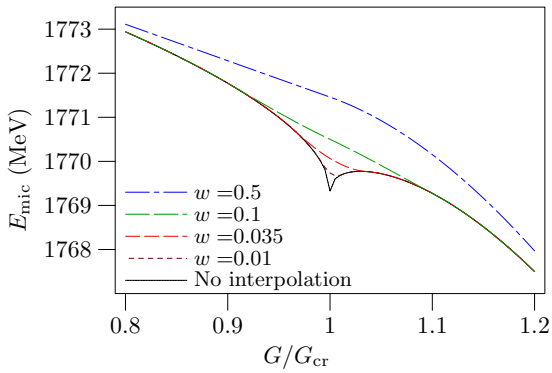

FIG. 7. Interpolated microscopic energy $E_{\rm mic}$ as a function of $G/G_{\rm cr}$ for different interpolation widths w in the case of ^{100}Sn. See the text for details.

This diminishing of w relative to the calculations in Refs. [10,12] has implications for the calculated "Wigner x," defined by [29]

$$E(N,Z) = E_0 + \frac{|M_T|(|M_T|+x)}{2\theta} + a_c \frac{Z(Z-1)}{A^{1/3}} B_c \quad (49)$$

for a constant A and $|M_T| = 0, 2, 4$ when $A \equiv 0 \mod 4$ and $1, 3, 5$ when $A \equiv 2 \mod 4$. Here, besides x, also E_0 and θ are constants. The value of a_c is the one that results from the fit of liquid-drop parameters described in Sec. II A. As a function of A the empirical x has local maxima at the mass numbers of the doubly magic nuclei ^{40}Ca, ^{56}Ni, and ^{100}Sn. This is seen in Fig. 8 (and also in the plots of x in Refs. [10,12], which resemble the bottom panel in Fig. 8 in this respect) to be reproduced with $w = 0.035$ but not with $w = 0.5$. The small w is similarly decisive for the sharpness of the calculated shell correction minimum at ^{100}Sn in the lower-right panel of Fig. 4. These successes of the small w in reproducing qualitative features of the patterns of binding energies near closed shells should evidently not be seen as a proof that it best approximates the exact minimum of the Hamiltonian (7).

VII. SUMMARY

The random-phase-approximation–amended (RPA-amended) Nilsson–Strutinskij method of calculating nuclear binding energies was reviewed in the form it has taken after

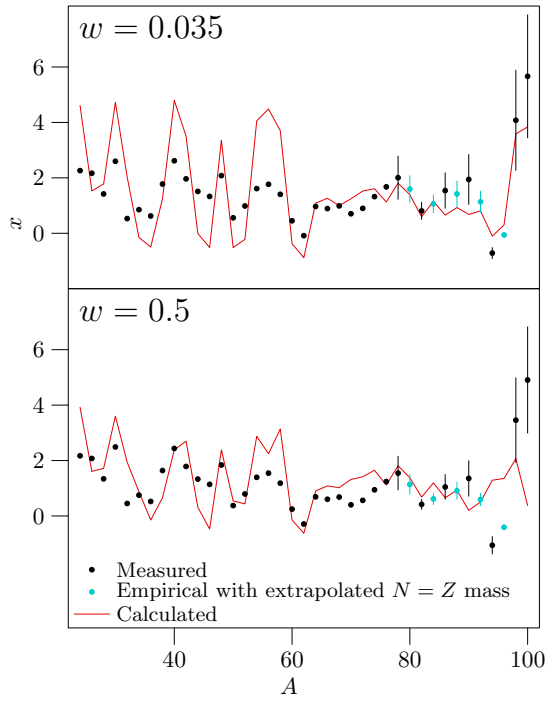

FIG. 8. The calculated Wigner x as a function of A for two different interpolation widths w in comparison with the values extracted from mass data. In both calculations, the pair coupling constants G_τ are those of Sec. III. The liquid drop parameters are optimized separately for $w = 0.5$, resulting in $(a_v, a_{vt}, a_s, a_{st}, a_c) =$ (14.98, 102.6, 15.82, 119.5, 0.6400) MeV and rms deviations 0.735 and 0.948 MeV from the doubly odd data and doubly even masses, respectively. The empirical points differ between the panels due to different a_c.

modifications in the preceding literature and in our present work. It was then applied in a study of odd-mass nuclei. Three sets of such nuclei were considered. In terms of the numbers N and Z of neutrons and protons and the mass number $A = N + Z$ they are (i) the sequence of nuclei with $Z = N - 1$ and $25 \leqslant A \leqslant 99$; (ii) the odd-$A$ isotopes of In, Sn, and Sb with $46 \leqslant N \leqslant 92$; (iii) the odd-$A$ isotopes of Sr, Y, Zr, Nb, and Mo with $60 \leqslant N \leqslant 64$. An RPA-based part of the total shell correction which accounts for the pair-vibrational correlation energy was found to contribute significantly to the calculated odd-even mass differences, particularly in the light nuclei. In the upper *sd* shell it thus gives almost the entire odd-even mass differences for odd Z and about half of it for odd N. In the heavier part of the set (i) it is less significant and the contribution is negative for odd $N > 30$. In the sets (ii) and (iii) it is dominantly positive and makes up 6%–31% of the total calculated odd-even mass difference in various cases. These differences were explained qualitatively in terms of a closed expression for a smooth RPA counter term.

The coupling constants G_n, G_p, and G_{np} of neutron, proton, and neutron-proton pairing interactions were expressed by Eq. (9) in terms of the parameters $\overline{G}$, ζ, and α, which were set independently for regions of the chart of nuclei each containing one of the sets (i)–(iii) of odd-A nuclei. In region (i), following previous studies of even-A nuclei in this region, we took $\alpha = 0$ and adjusted $\overline{G}$ and ζ to data on doubly odd nuclei with $N = Z$. Remarkably, the resulting parameters reproduce the typical size of the odd-even mass difference. In the regions (ii) and (iii) the parameters $\overline{G}$ and α were fit directly to the odd-even mass differences with ζ kept from region (i). Essentially the same $\overline{G}$ but different α resulted. The value of $\overline{G}$ derived from the data on doubly odd $N = Z$ nuclei is 24% greater than the one derived from odd-even mass differences in the regions (ii) and (iii). As a result we got for ^{100}Sn, which belongs to both regions (i) and (ii), two values of the common value of G_n, G_p, and G_{np} differing by these 24%. It was suggested that this difference be due to uncertainty of a part of the data on doubly odd $N = Z$ nuclei.

An investigation of the binding energies of the Sn isotopes with even N showed that our model reproduces a discontinuity of the two-neutron separation energy at $N = 66$ discussed recently by Togashi *et al.* [28]. Like in their analysis of results of a large-scale shell-model calculation, it is associated in our calculation with an onset of oblate deformations at the entrance of the $1h_{11/2}$ neutron shell. Pairing was found to contribute to the formation of the discontinuity.

The RPA neutron-proton pair-vibrational correlation energy is expected to decrease numerically with increasing neutron excess due to an increasing mismatch of the occupations of single-neutron and single-proton levels. In ^{142}Sn, which has almost twice as many neutrons as protons, it was found to be reduced anyway only to about two thirds of its value in the $N = Z$ nucleus ^{100}Sn.

The RPA-amended Nilsson–Strutinskij method involves an interpolation of RPA energy terms across the thresholds of the pair coupling constants for Bardeen–Cooper–Schrieffer pairing in the neutron or proton system. Arguments were given for choosing the interpolation interval substantially smaller than in previous applications of the method, and such a smaller width was applied in our present calculations. As a side effect, diminishing the width of the interpolation interval resulted in an improved qualitative correspondence between the variations with A of the measured and calculated Wigner x.

ACKNOWLEDGMENT

We would like to thank Stefan Frauendorf for providing access to the TAC code that was used to calculate the deformations shown in the Appendix and the corresponding single-nucleon levels used in this work.

APPENDIX: DEFORMATIONS

Table II shows the deformations used in the calculations. For odd $N = Z$ these are the deformations assumed for the lowest states with $T \approx 0$.

TABLE II. Deformations used in the calculations.

Nucleus	ϵ_2	γ (°)	ϵ_4	Nucleus	ϵ_2	γ (°)	ϵ_4	Nucleus	ϵ_2	γ (°)	ϵ_4	Nucleus	ϵ_2	γ (°)	ϵ_4	Nucleus	ϵ_2	γ (°)	ϵ_4
^{24}O	0.000		0.000	^{62}Fe	0.043	60	0.001	^{102}Zr	0.265	0	−0.002	^{101}In	0.026	0	0.005	^{135}Sn	0.013	60	−0.003
^{26}O	0.000		0.000	^{54}Co	0.084	0	0.007	^{103}Zr	0.266	0	0.005	^{103}In	0.036	0	0.005	^{136}Sn	0.000		0.000
^{24}Ne	0.091	0	0.000	^{56}Ni	0.000		0.000	^{104}Zr	0.270	0	0.010	^{105}In	0.053	0	0.004	^{137}Sn	0.009	60	−0.001
^{26}Ne	0.000		0.000	^{58}Ni	0.000		0.000	^{82}Nb	0.203	60	0.025	^{107}In	0.073	0	0.004	^{138}Sn	0.000		0.000
^{28}Ne	0.000		0.000	^{60}Ni	0.000		0.000	^{101}Nb	0.240	0	−0.006	^{109}In	0.082	0	0.005	^{139}Sn	0.000		0.000
^{30}Ne	0.000		0.000	^{62}Ni	0.000		0.000	^{103}Nb	0.257	0	0.000	^{111}In	0.082	0	0.007	^{140}Sn	0.000		0.000
^{24}Mg	0.284	0	0.014	^{64}Ni	0.000		0.000	^{105}Nb	0.263	10	0.011	^{113}In	0.082	0	0.007	^{141}Sn	0.012	0	0.000
^{26}Mg	0.201	0	0.012	^{66}Ni	0.000		0.000	^{84}Mo	0.200	60	0.031	^{115}In	0.104	36	0.002	^{142}Sn	0.000		0.000
^{28}Mg	0.000		0.000	^{58}Cu	0.054	0	−0.001	^{86}Mo	0.080	60	0.003	^{117}In	0.113	41	0.005	^{97}Sb	0.033	60	−0.004
^{30}Mg	0.000		0.000	^{60}Zn	0.000		0.000	^{88}Mo	0.000		0.000	^{119}In	0.107	2	0.009	^{99}Sb	0.026	60	−0.004
^{32}Mg	0.000		0.000	^{62}Zn	0.000		0.000	^{90}Mo	0.000		0.000	^{121}In	0.099	7	0.011	^{101}Sb	0.022	60	−0.004
^{34}Mg	0.000		0.000	^{64}Zn	0.000		0.000	^{92}Mo	0.000		0.000	^{123}In	0.080	7	0.011	^{103}Sb	0.026	60	−0.004
^{26}Al	0.223	30	0.002	^{66}Zn	0.037	60	0.001	^{94}Mo	0.000		0.000	^{125}In	0.051	0	0.008	^{105}Sb	0.035	60	−0.005
^{28}Si	0.222	60	−0.003	^{68}Zn	0.000		0.000	^{102}Mo	0.219	26	0.001	^{127}In	0.027	0	0.005	^{107}Sb	0.045	60	−0.005
^{30}Si	0.000		0.000	^{70}Zn	0.000		0.000	^{103}Mo	0.226	26	0.006	^{129}In	0.018	0	0.004	^{109}Sb	0.077	0	−0.012
^{32}Si	0.000		0.000	^{62}Ga	0.011	0	0.000	^{104}Mo	0.241	21	0.005	^{131}In	0.014	0	0.004	^{111}Sb	0.083	0	−0.009
^{34}Si	0.000		0.000	^{64}Ge	0.000		0.000	^{105}Mo	0.251	17	0.007	^{133}In	0.016	0	0.004	^{113}Sb	0.079	60	−0.007
^{36}Si	0.000		0.000	^{66}Ge	0.091	0	0.004	^{106}Mo	0.255	16	0.012	^{135}In	0.022	0	0.004	^{115}Sb	0.110	60	−0.009
^{38}Si	0.132	0	−0.005	^{68}Ge	0.113	60	0.002	^{86}Tc	0.189	57	0.034	^{137}In	0.033	0	0.003	^{117}Sb	0.126	60	−0.007
^{30}P	0.000		0.000	^{70}Ge	0.121	60	0.005	^{88}Ru	0.000		0.000	^{139}In	0.056	0	0.000	^{119}Sb	0.128	60	−0.002
^{32}S	0.000		0.000	^{72}Ge	0.000		0.000	^{90}Ru	0.000		0.000	^{141}In	0.086	0	−0.005	^{121}Sb	0.118	60	0.003
^{34}S	0.000		0.000	^{74}Ge	0.000		0.000	^{92}Ru	0.000		0.000	^{96}Sn	0.000		0.000	^{123}Sb	0.103	60	0.007
^{36}S	0.000		0.000	^{66}As	0.114	0	0.007	^{94}Ru	0.000		0.000	^{97}Sn	0.014	0	0.002	^{125}Sb	0.085	60	0.008
^{38}S	0.000		0.000	^{68}Se	0.171	60	−0.002	^{96}Ru	0.000		0.000	^{98}Sn	0.000		0.000	^{127}Sb	0.051	60	0.001
^{40}S	0.000		0.000	^{70}Se	0.213	60	−0.002	^{98}Ru	0.000		0.000	^{99}Sn	0.022	0	0.005	^{129}Sb	0.026	60	−0.002
^{42}S	0.000		0.000	^{72}Se	0.200	60	0.002	^{90}Rh	0.008	0	0.000	^{100}Sn	0.000		0.000	^{131}Sb	0.017	60	−0.003
^{34}Cl	0.054	60	0.003	^{74}Se	0.190	60	0.008	^{92}Pd	0.000		0.000	^{101}Sn	0.018	60	−0.002	^{133}Sb	0.014	60	−0.003
^{36}Ar	0.000		0.000	^{76}Se	0.000		0.000	^{94}Pd	0.000		0.000	^{102}Sn	0.000		0.000	^{135}Sb	0.016	60	−0.003
^{38}Ar	0.000		0.000	^{78}Se	0.058	0	0.000	^{96}Pd	0.000		0.000	^{103}Sn	0.011	60	−0.001	^{137}Sb	0.022	60	−0.004
^{40}Ar	0.000		0.000	^{70}Br	0.244	60	−0.004	^{98}Pd	0.000		0.000	^{104}Sn	0.000		0.000	^{139}Sb	0.033	60	−0.005
^{42}Ar	0.000		0.000	^{72}Kr	0.273	60	−0.003	^{100}Pd	0.000		0.000	^{105}Sn	0.000		0.000	^{141}Sb	0.066	0	−0.016
^{44}Ar	0.000		0.000	^{74}Kr	0.248	60	0.001	^{94}Ag	0.032	0	0.004	^{106}Sn	0.000		0.000	^{143}Sb	0.096	0	−0.020
^{46}Ar	0.000		0.000	^{76}Kr	0.220	60	0.008	^{94}Cd	0.000		0.000	^{107}Sn	0.015	0	0.001	^{98}Te	0.000		0.000
^{38}K	0.018	60	0.000	^{78}Kr	0.201	60	0.014	^{96}Cd	0.000		0.000	^{108}Sn	0.000		0.000	^{100}Te	0.000		0.000
^{40}Ca	0.000		0.000	^{80}Kr	0.063	0	0.001	^{98}Cd	0.000		0.000	^{109}Sn	0.009	60	−0.001	^{102}Te	0.000		0.000
^{42}Ca	0.000		0.000	^{82}Kr	0.051	0	0.002	^{100}Cd	0.000		0.000	^{110}Sn	0.000		0.000	^{104}Te	0.000		0.000
^{44}Ca	0.000		0.000	^{74}Rb	0.231	60	0.002	^{102}Cd	0.000		0.000	^{111}Sn	0.009	0	0.000	^{106}Te	0.000		0.000
^{46}Ca	0.000		0.000	^{76}Sr	0.238	60	0.006	^{104}Cd	0.000		0.000	^{112}Sn	0.000		0.000	^{108}Te	0.000		0.000
^{48}Ca	0.000		0.000	^{78}Sr	0.218	60	0.013	^{106}Cd	0.000		0.000	^{113}Sn	0.029	0	0.001	^{110}Te	0.000		0.000
^{50}Ca	0.000		0.000	^{80}Sr	0.205	60	0.018	^{108}Cd	0.084	0	0.003	^{114}Sn	0.000		0.000	^{112}Te	0.000		0.000
^{42}Sc	0.066	60	−0.008	^{82}Sr	0.073	60	0.003	^{110}Cd	0.086	0	0.005	^{115}Sn	0.068	60	−0.004	^{114}Te	0.000		0.000
^{44}Ti	0.000		0.000	^{84}Sr	0.000		0.000	^{112}Cd	0.092	0	0.006	^{116}Sn	0.000		0.000	^{116}Te	0.111	60	−0.009
^{46}Ti	0.000		0.000	^{86}Sr	0.000		0.000	^{114}Cd	0.122	60	−0.001	^{117}Sn	0.061	60	−0.001	^{118}Te	0.132	60	−0.007
^{48}Ti	0.000		0.000	^{98}Sr	0.248	60	−0.019	^{116}Cd	0.127	60	0.004	^{118}Sn	0.092	60	0.000	^{120}Te	0.132	60	−0.002
^{50}Ti	0.000		0.000	^{99}Sr	0.266	0	−0.007	^{118}Cd	0.116	60	0.009	^{119}Sn	0.088	60	0.001	^{122}Te	0.119	60	0.003
^{52}Ti	0.000		0.000	^{100}Sr	0.252	60	−0.013	^{120}Cd	0.111	4	0.013	^{120}Sn	0.088	60	0.004	^{124}Te	0.100	60	0.008
^{54}Ti	0.000		0.000	^{101}Sr	0.251	60	−0.008	^{122}Cd	0.084	29	0.012	^{121}Sn	0.083	60	0.006	^{126}Te	0.076	60	0.008
^{46}V	0.046	0	−0.004	^{102}Sr	0.249	60	−0.003	^{124}Cd	0.000		0.000	^{122}Sn	0.076	60	0.007	^{128}Te	0.000		0.000
^{48}Cr	0.150	0	−0.014	^{78}Y	0.222	60	0.013	^{126}Cd	0.000		0.000	^{123}Sn	0.064	60	0.007	^{130}Te	0.000		0.000
^{50}Cr	0.100	0	−0.002	^{99}Y	0.237	60	−0.015	^{128}Cd	0.000		0.000	^{124}Sn	0.039	60	0.003	^{132}Te	0.000		0.000
^{52}Cr	0.000		0.000	^{101}Y	0.265	0	−0.003	^{130}Cd	0.000		0.000	^{125}Sn	0.019	60	0.001	^{134}Te	0.000		0.000

TABLE II. (*Continued.*)

Nucleus	ϵ_2	γ (°)	ϵ_4	Nucleus	ϵ_2	γ (°)	ϵ_4	Nucleus	ϵ_2	γ (°)	ϵ_4	Nucleus	ϵ_2	γ (°)	ϵ_4	Nucleus	ϵ_2	γ (°)	ϵ_4
^{54}Cr	0.000		0.000	^{103}Y	0.241	60	0.000	^{132}Cd	0.000		0.000	^{126}Sn	0.000		0.000	^{136}Te	0.000		0.000
^{56}Cr	0.000		0.000	^{80}Zr	0.212	60	0.020	^{134}Cd	0.000		0.000	^{127}Sn	0.018	60	0.001	^{138}Te	0.000		0.000
^{58}Cr	0.087	0	0.002	^{82}Zr	0.204	60	0.025	^{136}Cd	0.000		0.000	^{128}Sn	0.000		0.000	^{140}Te	0.000		0.000
^{50}Mn	0.149	0	−0.005	^{84}Zr	0.153	60	0.016	^{138}Cd	0.000		0.000	^{129}Sn	0.016	60	0.001	^{142}Te	0.000		0.000
^{52}Fe	0.000		0.000	^{86}Zr	0.000		0.000	^{140}Cd	0.093	0	−0.009	^{130}Sn	0.000		0.000	^{144}Te	0.086	0	−0.014
^{54}Fe	0.000		0.000	^{88}Zr	0.000		0.000	^{95}In	0.037	0	0.006	^{131}Sn	0.019	0	0.006				
^{56}Fe	0.000		0.000	^{90}Zr	0.000		0.000	^{97}In	0.028	0	0.006	^{132}Sn	0.000		0.000				
^{58}Fe	0.000		0.000	^{100}Zr	0.249	0	−0.009	^{98}In	0.040	0	0.009	^{133}Sn	0.016	60	−0.004				
^{60}Fe	0.000		0.000	^{101}Zr	0.259	0	−0.006	^{99}In	0.022	0	0.005	^{134}Sn	0.000		0.000				

[1] J. Bardeen, L. N. Cooper, and J. R. Schrieffer, Phys. Rev. **106**, 162 (1957); **108**, 1175 (1957).
[2] A. Bohr, B. R. Mottelson, and D. Pines, Phys. Rev. **110**, 936 (1958).
[3] N. N. Bogolyubov, Dokl. Akad. Nauk SSSR **119**, 52 (1958) [Sov. Phys. Dokl. **3**, 279 (1958)].
[4] V. G. Solov'yov, Dokl. Akad. Nauk SSSR **123**, 437 (1958) [Sov. Phys. Dokl. **3**, 1176 (1958)]; Dokl. Akad. Nauk SSSR **123**, 652 (1958) [Sov. Phys. Dokl. **3**, 1197 (1958)].
[5] J. Bang and J. Krumlinde, Nucl. Phys. A **141**, 18 (1970).
[6] R. W. Richardson, Phys. Lett. **3**, 277 (1963).
[7] D. Bohm and D. Pines, Phys. Rev. **92**, 609 (1953).
[8] V. M. Strutinskij, Yad. Fiz. **3**, 614 (1966) [Sov. J. Nucl. Phys. **3**, 449 (1966)].
[9] K. Neergård, Phys. Rev. C **80**, 044313 (2009).
[10] I. Bentley, K. Neergård, and S. Frauendorf, Phys. Rev. C **89**, 034302 (2014).
[11] K. Neergård, Phys. Rev. C **94**, 054328 (2016).
[12] K. Neergård, Nucl. Theor. **36**, 195 (2017).
[13] I. Bentley, Ph.D. thesis, University of Notre Dame, 2010 (unpublished).
[14] S. G. Nilsson, C. F. Tsang, A. Sobiczewski, Z. Szymanski, S. Wycech, C. Gustafson, I. L. Lamm, P. Möller, and B. Nilsson, Nucl. Phys. A **131**, 1 (1969).
[15] S. A. Larsson, Phys. Scr. **8**, 17 (1973).
[16] P. A. Seeger and W. M. Howard, Nucl. Phys. A **238**, 491 (1975).
[17] A. R. Edmonds, *Angular Momentum in Quantum Mechanics* (Princeton University Press, Princeton, 1957).
[18] W. J. Swiatecki, Phys. Rev. **104**, 993 (1956).
[19] S. G. Nilsson, Mat. Fys. Medd. Dan. Vid. Selsk. **29**, 16 (1955).
[20] T. Bengtsson and I. Ragnarsson, Nucl. Phys. A **436**, 14 (1985).
[21] P. Ring and P. Schuck, *The Nuclear Many-Body Problem* (Springer, Berlin, 1980).
[22] V. M. Strutinsky, Nucl. Phys. A **95**, 420 (1967).
[23] N. Hinohara and W. Nazarewicz, Phys. Rev. Lett. **116**, 152502 (2016).
[24] N. L. Vaquero, J. L. Egido, and T. R. Rodríguez, Phys. Rev. C **88**, 064311 (2013).
[25] G. Audi, M. Wang, A. H. Wapstra, F. G. Kondev, M. MacCormick, X. Xu, and P. Pfeiffer, Ch. Phys. C **36**, 1287 (2012).
[26] V. J. Huang, G. Audi, M. Wang, F. G. Kondev, S. Naimi, and X. Xu, Ch. Phys. C **41**, 030002 (2017).
[27] Evaluated Nuclear Structure Data File, https://www.nndc.bnl.gov/ensdf, data retrieved Nov. 1, 2018.
[28] T. Togashi, Y. Tsunoda, T. Otsuka, N. Shimizu, and M. Honma, Phys. Rev. Lett. **121**, 062501 (2018).
[29] I. Bentley and S. Frauendorf, Phys. Rev. C **88**, 014322 (2013).
[30] J. Högaasen-Feldman, Nucl. Phys. **28**, 258 (1961).
[31] J. Dukelsky, V. G. Gueorguiev, P. Van Isacker, S. Dimitrova, B. Errea, and S. Lerma H., Phys. Rev. Lett. **96**, 072503 (2006).